

# Planar Hall Effect in Quasi-Two-Dimensional Materials

Koushik Ghorai,\* Sunit Das,\* Harsh Varshney, and Amit Agarwal†  
*Department of Physics, Indian Institute of Technology Kanpur, Kanpur-208016, India*

The planar Hall effect in 3D systems is an effective probe for their Berry curvature, topology, and electronic properties. However, the Berry curvature-induced conventional planar Hall effect is forbidden in 2D systems as the out-of-plane Berry curvature cannot couple to the band velocity of the electrons moving in the 2D plane. Here, we demonstrate a unique 2D planar Hall effect (2DPHE) originating from the hidden planar components of the Berry curvature and orbital magnetic moment in quasi-2D materials. We identify all planar band geometric contributions to 2DPHE and classify their crystalline symmetry restrictions. Using gated bilayer graphene as an example, we show that in addition to capturing the hidden band geometric effects, 2DPHE is also sensitive to the Lifshitz transitions. Our work motivates further exploration of hidden planar band geometry-induced 2DPHE and related transport phenomena for innovative applications.

The planar Hall effect (PHE) is the generation of longitudinal and transverse voltages in the plane of the applied electric ( $\mathbf{E}$ ) and magnetic fields ( $\mathbf{B}$ ). In contrast to the conventional and anomalous Hall effect, the transport in PHE is dissipative, and the response typically varies quadratically with the  $B$ . PHE has extensive applications in magnetic sensors and memory devices [1]. In 3D materials, PHE generally originates from the coupling of the Berry curvature (BC) and orbital magnetic moment (OMM) to the band velocity and in-plane magnetic field, which generates a longitudinal and transverse planar response. Initial studies of PHE used it effectively to probe the magnetization reversal in magnetic materials [2–6]. More recently, we have used PHE to explore novel topological semimetals [7–17] and topological insulators [18, 19].

However, conventional PHE probes are ineffective in 2D systems. As the 2D plane confines the orbital motion of electrons, these systems can host only out-of-plane Berry curvature and orbital magnetic moment [20, 21]. Consequently, the PHE induced by the component of the BC and OMM along the applied in-plane magnetic field is forbidden in perfect 2D systems. Some 2D materials with strong spin-orbit coupling exhibit an intrinsic magnetohall response driven by magnetic field-induced changes to the Berry curvature [22–28]. However, such responses are antisymmetric tensors and absent in systems lacking strong spin-orbit interactions. These limitations severely restrict our ability to utilize PHE to explore fundamental physics and develop ultra-sensitive magnetic sensors and other applications in 2D materials.

In this Letter, we introduce a unique 2D planar Hall effect (2DPHE) in layered 2D materials such as bilayer graphene. Layered 2D materials with finite inter-layer tunneling can host an intrinsic in-plane component of the BC and OMM if the system’s space inversion or time-reversal symmetry is broken [29–31]. We demonstrate that these relatively unexplored in-plane components of the band geometric quantities induce the 2DPHE response (see Fig. 1). We present a thorough analysis of the 2DPHE responses, particularly their angular varia-

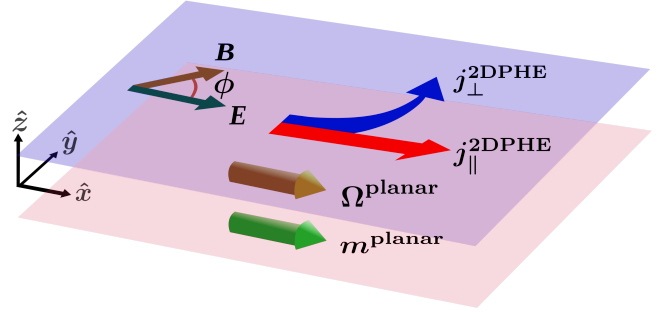


FIG. 1. Schematic for 2D planar Hall effect (2DPHE). Layered 2D materials host hidden planar Berry curvature ( $\Omega^{\text{planar}}$ ) and planar orbital magnetic moment ( $\mathbf{m}^{\text{planar}}$ ) arising from inter-layer tunneling. The  $\Omega^{\text{planar}}$  and  $\mathbf{m}^{\text{planar}}$  combine with the in-plane electric and magnetic field to induce a longitudinal and transverse current in the 2D plane.

tion (angle between  $\mathbf{E}$  and  $\mathbf{B}$ ), and classify the crystalline symmetry restrictions on the different 2DPHE response tensors. As an illustrative example, we focus on Bernal stacked bilayer graphene to demonstrate a sizable and gate-tunable 2DPHE response. Beyond predicting the unique phenomena of 2DPHE, our findings motivate the exploration of other transport and optical phenomena induced by the hidden planar band geometric quantities in layered 2D materials [32].

*Planar-BC and OMM in 2D systems:*– In quasi-2D materials with two or more atomic layers, the finite inter-layer hopping amplitude enables the inter-layer tunneling of electrons. The inter-layer coherence of the electron wavefunction gives rise to hidden planar components of the BC and OMM. These are given by,

$$\Omega_{n\mathbf{k}}^{\text{planar}} = 2\hbar \text{Re} \sum_{n' \neq n} \frac{\mathbf{v}_{nn'} \times \mathbf{z}_{n'n}}{(\varepsilon_{n\mathbf{k}} - \varepsilon_{n'\mathbf{k}})}, \quad (1)$$

$$\mathbf{m}_{n\mathbf{k}}^{\text{planar}} = e \text{Re} \sum_{n' \neq n} \mathbf{v}_{nn'} \times \mathbf{z}_{n'n}. \quad (2)$$

Here, we have defined the velocity matrix elements as  $\hbar\mathbf{v}_{nn'} = \langle u_{n\mathbf{k}} | \nabla_{\mathbf{k}} \mathcal{H} | u_{n'\mathbf{k}} \rangle$ , with  $\mathbf{k} = (k_x, k_y)$ .  $\varepsilon_{n\mathbf{k}}$  and

TABLE I. The symmetry restrictions of the longitudinal and planar Hall response tensors pertaining to two-dimensional materials. The cross ( $\times$ ) and the tick ( $\checkmark$ ) mark signify the corresponding response tensor is symmetry forbidden and allowed, respectively. The longitudinal and transverse PHE tensors in the same row have identical symmetry restrictions.

Longitudinal	Transverse	$\mathcal{P}$	$\mathcal{T}$	$\mathcal{PT}$	$\mathcal{M}_x$	$\mathcal{M}_y$	$\mathcal{M}_z$	$\mathcal{C}_{2x}$	$\mathcal{C}_{2y}$	$\mathcal{C}_{2z}$	$\mathcal{C}_{3z}$	$\mathcal{C}_{4z}$	$\mathcal{C}_{6z}$	$\mathcal{S}_{4z}$	$\mathcal{S}_{6z}$
$\chi_{xx;x}$	$\chi_{yx;y}$	$\checkmark$	$\times$	$\times$	$\checkmark$	$\times$	$\times$	$\checkmark$	$\times$	$\times$	$\checkmark$	$\times$	$\times$	$\times$	$\checkmark$
$\chi_{xx;y}$	$\chi_{yx;x}$	$\checkmark$	$\times$	$\times$	$\times$	$\checkmark$	$\times$	$\times$	$\checkmark$	$\times$	$\checkmark$	$\times$	$\times$	$\times$	$\checkmark$
$\chi_{xx;xx}, \chi_{xx;yy}$	$\chi_{yx;xy}$	$\checkmark$	$\checkmark$	$\checkmark$	$\checkmark$	$\checkmark$	$\checkmark$	$\checkmark$	$\checkmark$	$\checkmark$	$\checkmark$	$\checkmark$	$\checkmark$	$\checkmark$	$\checkmark$
$\chi_{xx;xy}$	$\chi_{yx;xx}, \chi_{yx;yy}$	$\checkmark$	$\checkmark$	$\checkmark$	$\times$	$\times$	$\checkmark$	$\times$	$\times$	$\checkmark$	$\checkmark$	$\checkmark$	$\checkmark$	$\checkmark$	$\checkmark$

$|u_{n\mathbf{k}}\rangle$  are the band energy and periodic part of the Bloch wavefunction for the  $n$ -th band, respectively. The matrix elements of the out-of-plane position operator are defined as  $\mathcal{Z}_{nn'} = \hat{z} \langle u_{n\mathbf{k}} | \mathcal{Z} | u_{n'\mathbf{k}} \rangle$ , with  $\mathcal{Z}$  being the position operator along the  $\hat{z}$ -direction. These in-plane contributions combined with the conventional out-of-plane components yield the total BC and OMM for quasi-2D materials. We present the detailed derivation of these equations in Sec. S1 of the Supplementary Materials (SM) [33]. We emphasize that the planar-BC and planar-OMM rely on inter-layer hybridization of electronic states, which makes the off-diagonal components of  $\mathcal{Z}_{nn'}$  finite. We illustrate the emergence of the planar-BC and OMM and their symmetry properties in an intuitive way using a  $2 \times 2$  low energy model [6, 34] Hamiltonian of bilayer graphene in Sec. S2 of the SM [33].

*2D Planar Hall effect:*— In 2D systems, generally, the magnetic field interacts with electrons primarily through Zeeman coupling to its spin [22–26, 28]. In contrast, the planar-OMM allows the magnetic field to couple directly to the orbital motion of electrons. This modifies the band energy ( $\tilde{\varepsilon}_{n\mathbf{k}} = \varepsilon_{n\mathbf{k}} - \mathbf{m}_{n\mathbf{k}}^{\text{planar}} \cdot \mathbf{B}$ ) and the band velocity. More importantly, the planar-BC combines with the band velocity to generate a finite chiral magnetic velocity [35] in 2D systems, which is  $\propto (\mathbf{v}_{n\mathbf{k}} \cdot \boldsymbol{\Omega}_{n\mathbf{k}}^{\text{planar}}) \mathbf{B}$ . We show below that these magnetic field-dependent velocity contributions arising from the hidden planar-BC and -OMM generate a previously unexplored planar Hall effect in 2D systems.

In the semiclassical Boltzmann transport framework, the charge current is given by  $\mathbf{j} = -e \sum_n \int [d\mathbf{k}] \dot{\mathbf{r}}_n g_{n\mathbf{k}}$ . Here  $g_{n\mathbf{k}}$  is the non-equilibrium distribution function,  $\dot{\mathbf{r}}_n$  is the wave-packet velocity, and  $[d\mathbf{k}] \equiv d^2\mathbf{k}/(2\pi)^2$  for 2D systems. Using the expressions of the planar-BC and OMM modified  $\dot{\mathbf{r}}_n$  and  $g_{n\mathbf{k}}$  up to linear order in the applied electric field, we calculate the planar current density to the first and second orders in the magnetic field strength  $B$ . See Sec. S3 of the SM for a detailed derivation [33]. We obtain the longitudinal and transverse components of the 2DPHE currents to be

$$j_a = \tau \chi_{ab;c} E_b B_c + \tau \chi_{ab;cd} E_b B_c B_d. \quad (3)$$

Here,  $\tau$  is the electron scattering time,  $\{a, b, c, d\} \in \{x, y\}$  are the 2D Cartesian coordinates, and the Einstein sum-

mation convention is used. In Eq. (3),  $\chi_{ab;cd}$  is symmetric under the exchange of magnetic field indices ( $c, d$ ). The 2DPHE response tensors can be expressed as a sum of the planar-BC, planar-OMM, and mixed terms,

$$\chi_{ab;c(d)} = \chi_{ab;c(d)}^{\text{BC}} + \chi_{ab;c(d)}^{\text{OMM}} + \chi_{ab;c(d)}^{\text{BC+OMM}}. \quad (4)$$

We obtain the planar-BC contributions to be

$$\begin{aligned} \chi_{ab;c}^{\text{BC}} &= -e^2 \int_{n,\mathbf{k}} [(v_a \delta_{bc} + v_b \delta_{ac}) \Omega_V - \frac{e}{\hbar} v_a v_b \Omega_c] f'_0, \quad (5) \\ \chi_{ab;cd}^{\text{BC}} &= -\frac{e^2}{2} \int_{n,\mathbf{k}} \left[ \delta_{ad} \delta_{bc} \Omega_V^2 - \frac{e}{\hbar} (v_a \delta_{bc} + v_b \delta_{ac}) \Omega_d \Omega_V \right. \\ &\quad \left. + \frac{e^2}{\hbar^2} v_a v_b \Omega_c \Omega_d \right] f'_0 + (c \leftrightarrow d). \quad (6) \end{aligned}$$

Here,  $\Omega_V \equiv (e/\hbar) \mathbf{v}_{\mathbf{k}} \cdot \boldsymbol{\Omega}_{\mathbf{k}}$  with  $\hbar \mathbf{v}_{\mathbf{k}} = \nabla_{\mathbf{k}} \varepsilon_{\mathbf{k}}$  being the band velocity without any magnetic field, and  $\delta_{ab}$  is the Kronecker delta function. For brevity, we have defined  $\int_{n,\mathbf{k}} \equiv \sum_n \int [d\mathbf{k}]$ , and we do not explicitly mention the band index  $n$  in the physical quantities. Both of these linear and quadratic  $B$  conductivity tensors are  $\propto f'_0 \equiv \partial_\varepsilon f_0$ , highlighting that these 2DPHE responses are Fermi surface effect. We present the expressions for other contributions in Eq. (4) in Sec. S3 of the SM [33].

The planar response tensors in Eqs. (5) and (6) are proportional to either  $\mathbf{v}_{\mathbf{k}} \cdot \boldsymbol{\Omega}_{\mathbf{k}}$  or,  $\hat{\mathbf{B}} \cdot \boldsymbol{\Omega}_{\mathbf{k}}$  or, the combination of these terms. For a quasi-2D system, all of these terms vanish if we consider only the conventional out-of-plane BC. As a consequence, earlier works missed this phenomena. This highlights the crucial role of the hidden planar-BC and -OMM in generating the PHE response in quasi-2D systems. Furthermore, the response tensors  $\chi_{ab;c}$  and  $\chi_{ab;cd}$  are symmetric with respect to its first two indices. Therefore, we have  $\sum_a j_a E_a \neq 0$ , indicating the dissipative nature of the planar Hall current. Having established the possibility of 2DPHE, we now analyze the restrictions imposed by crystalline point group symmetries on different 2DPHE response tensors.

*Crystal symmetry restrictions:*— The inversion symmetry ( $\mathcal{P}$ ) imposes no constraints as both  $\chi_{ab;c}$  and  $\chi_{ab;cd}$  represent linear in  $E$  responses. However, under time-reversal ( $\mathcal{T}$ ) operation,  $j$ ,  $B$ , and  $\tau$  reverse signs, while  $E$  is  $\mathcal{T}$  even. Thus,  $\chi_{ab;c}$  is a third rank  $\mathcal{T}$ -odd axial tensor [36, 37], which is forbidden in non-magnetic systems

(see Sec. S4 of SM [33] for details). In contrast,  $\chi_{ab;cd}$  is a fourth rank  $\mathcal{T}$ -even polar tensor and is the leading order contribution in non-magnetic systems. Denoting a general point group operation via  $\mathcal{O}$ , the  $\chi_{ab;c}$  and  $\chi_{ab;cd}$  tensors obey the following transformation rules [36]

$$\chi_{a'b';c'} = \eta_{\mathcal{T}} \det\{\mathcal{O}\} \mathcal{O}_{a'a} \mathcal{O}_{b'b} \mathcal{O}_{c'c} \chi_{ab;c}, \quad (7)$$

$$\chi_{a'b';c'd'} = \mathcal{O}_{a'a} \mathcal{O}_{b'b} \mathcal{O}_{c'c} \mathcal{O}_{d'd} \chi_{ab;cd}. \quad (8)$$

Here,  $\eta_{\mathcal{T}} = \pm 1$  is associated with the magnetic point group symmetry transformation:  $\eta_{\mathcal{T}} = -1$  ( $\eta_{\mathcal{T}} = 1$ ) for magnetic (non-magnetic) point group operation  $\mathcal{O} \equiv \mathcal{RT}$  ( $\mathcal{O} \equiv \mathcal{R}$ ), with  $\mathcal{R}$  being a spatial operation.

To be specific about the symmetry constraints of the 2DPHE response, we apply the  $\mathbf{E}$  along  $\hat{x}$  direction, and an in-plane magnetic field at an angle  $\phi$  with  $\mathbf{E}$ , *i.e.*,  $(B_x, B_y) = B(\cos \phi, \sin \phi)$  (see Fig. 1). As the response tensors are symmetric in the first two indices, the independent tensor elements for the  $B$ -linear longitudinal (transverse) responses are  $\chi_{xx;x}$  and  $\chi_{xx;y}$  ( $\chi_{yx;x}$  and  $\chi_{yx;y}$ ). The fourth rank tensor  $\chi_{ab;cd}$  is symmetric in the first two ( $a, b$ ) and the last two ( $c, d$ ) indices. Hence, for the quadratic- $B$  longitudinal (transverse) response  $\chi_{xx;xx}$ ,  $\chi_{xx;yy}$  and  $\chi_{xx;xy}$  ( $\chi_{yx;xx}$ ,  $\chi_{yx;yy}$  and  $\chi_{yx;xy}$ ) are the only independent elements. We present crystalline symmetry imposed restrictions on these tensor elements for non-magnetic and magnetic systems in Table I and Table S1 of SM [33], respectively. An interesting conclusion from our symmetry analysis is that the presence of  $\mathcal{C}_{3z}$  symmetry does not restrict any of the 2DPHE response tensors. This makes hexagonal systems such as multi-layered graphene, transition metal dichalcogenides, and their twisted moiré heterostructures good candidates to observe 2DPHE. We note that the crystal symmetry restrictions discussed above are necessary but not sufficient conditions for the existence of different 2DPHE response tensors. We now focus on the angular variation of the 2DPHE current.

*Angular variation of the 2DPHE currents:*– The variation of the 2DPHE currents with the planar angle between the  $\mathbf{E}$  and  $\mathbf{B}$ , is important for exploring its origin and the relative contribution of different terms. We work with the field configuration described in Fig. 1 to obtain the longitudinal and transverse 2DPHE currents:  $j_{\parallel(\perp)}^{2\text{DPHE}} = \sigma^{\parallel(\perp)} E_{\parallel}$ . We calculate the angular dependence of the 2DPHE conductivities to be,

$$\sigma^{\parallel} = \tau B (\chi_{xx;x} \cos \phi + \chi_{xx;y} \sin \phi) + \tau B^2 (\chi_{xx;xx} \cos^2 \phi + \chi_{xx;yy} \sin^2 \phi + \chi_{xx;xy} \sin \phi \cos \phi), \quad (9)$$

$$\sigma^{\perp} = \tau B (\chi_{yx;x} \cos \phi + \chi_{yx;y} \sin \phi) + \tau B^2 (\chi_{yx;xx} \cos^2 \phi + \chi_{yx;yy} \sin^2 \phi + \chi_{yx;xy} \sin \phi \cos \phi). \quad (10)$$

These equations and the symmetry restrictions in Table I (and Table S1 in SM [33]) provide a complete characterization of the 2DPHE responses. For non-magnetic sys-

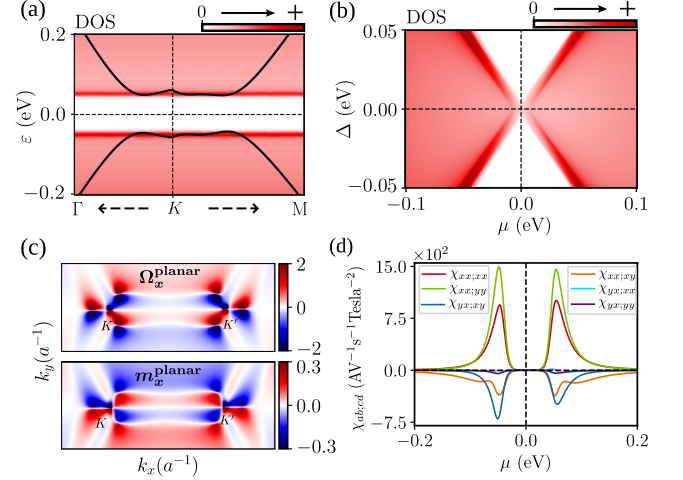


FIG. 2. (a) Electronic band structure of strained BLG around the  $K$  point, with the background color showing the density of states (DOS). (b) The variation of DOS with chemical potential  $\mu$  and the inter-layer potential  $\Delta$  in (b). The Van Hove singularity in the DOS near the band edges [also seen in (a)] is accompanied by a Lifshitz transition, where the system evolves from hosting three Fermi pockets around the  $K$  (or  $K'$ ) point to one Fermi pocket. (c) The upper (lower) panel shows the  $k$ -space distribution of the  $x$ -component of the planar BC (OMM) for the first conduction band in the unit of  $a^2$  ( $\frac{e}{h} a^2 \text{eV}$ ), where  $a$  is the lattice constant. (d) Different components of 2DPHE response tensors  $\chi_{ab;cd}$  as a function of  $\mu$  evaluated at temperature  $T = 50\text{K}$ . The peak in the response tensors coincides with the location of the Van Hove singularity in the DOS.

tems with an in-plane mirror or an in-plane two-fold rotation symmetry, the longitudinal (transverse) response is entirely captured by  $\chi_{xx;xx}$ , and  $\chi_{xx;yy}$  ( $\chi_{yx;xy}$ ) with the conventional  $\cos^2 \phi$  ( $\sin 2\phi$ ) angular dependence.

*2DPHE in gated bilayer graphene:*– To demonstrate the 2DPHE in a realistic system, we consider the tight-binding model of Bernal stacked bilayer graphene (BLG). It offers the natural advantage of being readily available, and its doping and layer asymmetry can be tuned via the combination of top and bottom gate voltages. The Hamiltonian of pristine BLG with a vertical displacement field possesses  $\mathcal{T}$  and  $\mathcal{C}_{3z}$  symmetry, while it breaks  $\mathcal{P}$  symmetry. Owing to the presence of  $\mathcal{T}$  symmetry in BLG, only the  $B^2$  contributions to the 2DPHE in BLG are allowed. The breakdown of  $\mathcal{P}$  symmetry is crucial for inducing a planar-BC and planar-OMM in systems with  $\mathcal{T}$  symmetry. BLG also has a mirror symmetry about its armchair direction, which we represent by  $\mathcal{M}_x$  (see Fig. S2 of SM [33]). The  $\mathcal{M}_x$  symmetry of BLG dictates that only the  $\chi_{yx;xy}$  component can be finite with the  $\sin 2\phi$  angular dependence in  $\sigma^{\perp}$ . To explore the role of other planar BC contributions  $\propto B^2$  ( $\chi_{yx;xx}$  and  $\chi_{yx;yy}$ ), we break the  $\mathcal{M}_x$  symmetry of BLG by applying a uniaxial strain of 1% strength at an angle of  $30^\circ$  to the zig-zag

direction. The details of the strain implementation in the tight-binding model of BLG are discussed in Sec. S5 of SM [33]. We present the band structure of strained BLG around one of the two valleys ( $K$  point) in Fig. 2(a). In Fig. 2(b), we show the color plot of the density of states as a function of the chemical potential ( $\mu$ ) and inter-layer potential ( $\Delta$ ).

For BLG, the out-of-plane position operator is given by the matrix  $\mathcal{Z} = \frac{c}{2}\sigma_0 \otimes \tau_z$ .  $\sigma_0$  is the identity matrix for the sublattice space, and  $\tau_z$  is the Pauli matrix in the layer space. Here,  $c \approx 3.35 \text{ \AA}$  is the inter-layer distance. We use this in Eqs. (1) and (2) to calculate the planar-BC and -OMM. We present the  $x$ -component of planar-BC and planar-OMM for the first conduction band in Fig. 2(c). The  $y$ -components of these quantities are presented in Sec. S5 of SM [33]. These quantities are not  $\mathcal{C}_{3z}$  symmetric even without any in-plane strain [31, 38]. However, they are valley contrasting due to the global  $\mathcal{T}$ -symmetry of BLG.

We numerically calculate the 2DPHE responses of BLG, illustrating their dependence on the chemical potential  $\mu$  in Fig. 2(d). In contrast to  $\chi_{xx;xx}$ ,  $\chi_{xx;yy}$ , and  $\chi_{yx;xy}$ , which remain finite even in the presence of  $\mathcal{M}_x$  symmetry, the contributions  $\chi_{xx;xy}$ ,  $\chi_{yx;xx}$ , and  $\chi_{yx;yy}$  require  $\mathcal{M}_x$  symmetry breaking to be finite. As a consequence, these contributions are relatively smaller in magnitude. We highlight that all the 2DPHE response tensors are pronounced in the vicinity of the band edges, where the planar band geometric quantities have a hotspot (see Fig. 2(c)). Interestingly, the peak in the responses near the band edge arises from the Van Hove singularity in the density of states, which is a marker of the Lifshitz transitions in BLG (see Sec. S6 of the SM [33] for more details).

We present color plots of the variation of  $\sigma^{\parallel}$  and  $\sigma^{\perp}$  with  $\mu$  and the inter-layer potential  $\Delta$  in Fig. 3(a) and 3(c). Both the conductivities have appreciable values only in the vicinity of the band edges, highlighting the band-geometric nature of 2DPHE. The peaks in both  $\sigma_{\perp}$  and  $\sigma_{\parallel}$  reflect the Van Hove singularity in the DOS, marked by the dark regions in Fig. 2(b). We present the angular variation of  $\sigma^{\parallel}$  and  $\sigma^{\perp}$ , as  $\mu$  is varied, in the polar color plots in Figs. 3(b) and 3(d). We highlight that the angular variation of the 2DPHE responses deviates from the conventional  $\sigma_{\parallel} \propto \cos^2 \phi$  and  $\sigma_{\perp} \propto \sin 2\phi$  dependence. This is a consequence of the strain-induced  $\mathcal{M}_x$  symmetry breaking, which makes  $\chi_{xx;xy}$ ,  $\chi_{yx;xx}$  and  $\chi_{yx;yy}$  components finite, modifying the angular dependence following Eqs. (9) and (10).

*Experimental implications:*— For estimating the feasibility of measuring 2DPHE responses in experiments, we consider an in-plane magnetic field of  $B = 1$  Tesla,  $\tau = 1$  ps, and  $\phi = 60^\circ$ . With these parameters,  $\sigma^{\perp}$  ( $\sigma^{\parallel}$ ) becomes  $\sim 0.1$  (4.5)  $\text{AV}^{-1}\text{m}^{-1}$  in BLG. Here, we have converted conductivities to the conventional 3D unit using the layer thickness of BLG. Assuming a sample size of

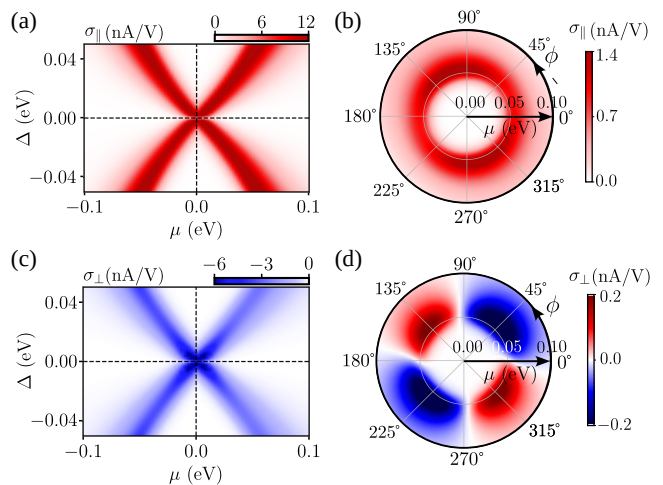


FIG. 3. The color plot of the (a) longitudinal and (c) transverse 2DPHE conductivities in  $\mu - \Delta$  space for strained BLG. These parameters can be experimentally tuned by the top and back gates. We have chosen the  $\tau = 1$  ps,  $B = 1$  Tesla,  $\phi = 60^\circ$  and temperature  $T = 50$  K. The angular dependence of the (b) longitudinal and (d) transverse 2DPHE conductivities. The small deviation from  $\sigma_{\parallel} \propto \cos^2 \phi$  and  $\sigma_{\perp} \propto \sin(2\phi)$  dependence is induced by the strain-induced mirror symmetry breaking. In the angular plots, we have  $\Delta = 0.05$  eV.

$\sim 10 \mu\text{m}$  and a moderate electric field of  $E \sim 1 \text{ V}/\mu\text{m}$ , we estimate the planar Hall voltage to be  $V_{\perp} \sim 0.17 \mu\text{V}$  (see Sec. S7 of SM [33]), which is well within experimental reach. Note that  $\Omega_{nk}^{\text{planar}}$  and  $m_{nk}^{\text{planar}}$  magnitude and hence the strength of 2DPHE responses increase with the number of layers. We show this explicitly for multi-layered graphene in Sec. S8 of SM [33].

We now explore ways to distinguish 2DPHE from other possible in-plane magneto-Hall responses (see Sec. S9 of SM [33] for details). The corrections in the anomalous Hall velocity generated by the magnetic field-induced Berry curvature can give rise to in-plane magneto-Hall responses  $\propto EB$  [22–26, 28]. The planar Hall effect can also arise from the anisotropic spin scattering mechanism [39–46]. All these in-plane magneto-Hall responses in 2D systems require strong spin-orbit coupling (SOC). Also, the responses are represented by the antisymmetric (symmetric) response tensors when they arise from the field-dependent anomalous velocity (anisotropic spin-scattering mechanism). In contrast, our proposed 2DPHE responses are symmetric and do not require SOC to be finite. Consequently, in a layered 2D system with SOC, such as transition metal dichalcogenides, the symmetrization of the total planar response will discard all antisymmetric contributions. The total symmetric planar response will have contributions from the 2DPHE and asymmetric spin scattering. However, the asymmetric spin scattering contribution is comparatively negligible in BLG due to its very small SOC strength. The

asymmetric spin-scattering-induced contribution can be differentiated by its unique double-peak structure around the charge-neutrality point [40, 44]. Beyond these responses, lock-in measurement techniques can easily distinguish 2DPHE from other nonlinear in-plane responses.

*Conclusion:*— Our discovery of 2DPHE brings the vast class of layered 2D materials under the purview of planar Hall effect probes, which were limited to 3D materials. Additionally, 2DPHE offers a novel tool to probe the previously unexplored planar quantum-geometric properties of Bloch electrons in 2D materials. The existence of planar Berry curvature and orbital magnetic moment motivates the study of other novel phenomena, which were believed to be inaccessible in 2D materials. For instance, the planar Berry curvature can give rise to a vertical (perpendicular to the 2D plane) anomalous Hall effect in the linear and nonlinear response regimes. An interesting application of this is that vertical charge transport, with restricted out-of-plane carrier velocity, can induce an inter-layer electric polarization. This may offer a novel way to control the switching of out-of-plane electric polarization in layered ferroelectric materials [47–49] via an in-plane electric field, with potential for new device applications. 2DPHE also enables the designing of highly sensitive planar Hall magnetic sensors using ultra-thin 2D materials. Our work opens new avenues for further exploration of novel transport effects and their potential applications arising from the hidden planar band geometric quantities.

*Acknowledgements:*— We acknowledge many fruitful discussions with Debottam Mandal (IIT Kanpur, India) and Atasi Chakraborty (Johannes Gutenberg University, Germany). KG, SD, and HV acknowledge the Ministry of Education, Government of India, for funding support through the Prime Minister’s Research Fellowship program.

---

\* KG and SD contributed equally and are joint first authors.

† [amitag@iitk.ac.in](mailto:amitag@iitk.ac.in)

- [1] L. K. Quynh, N. T. Hien, N. H. Binh, T. T. Dung, B. D. Tu, N. H. Duc, and D. T. H. Giang, Simple planar hall effect based sensors for low-magnetic field detection, *Advances in Natural Sciences: Nanoscience and Nanotechnology* **10**, 025002 (2019).
- [2] K. L. Yau and J. T. H. Chang, The planar hall effect in thin foils of ni-fe alloy, *Journal of Physics F: Metal Physics* **1**, 38–43 (1971).
- [3] J. Li, S. L. Li, Z. W. Wu, S. Li, H. F. Chu, J. Wang, Y. Zhang, H. Y. Tian, and D. N. Zheng, A phenomenological approach to the anisotropic magnetoresistance and planar hall effect in tetragonal  $\text{La}_2/3\text{Ca}_1/3\text{MnO}_3$  thin films, *Journal of Physics: Condensed Matter* **22**, 146006 (2010).
- [4] H. X. Tang, R. K. Kawakami, D. D. Awschalom, and M. L. Roukes, Giant planar hall effect in epitaxial (ga,mn)as devices, *Phys. Rev. Lett.* **90**, 107201 (2003).
- [5] M. Bowen, K.-J. Friedland, J. Herfort, H.-P. Schönherr, and K. H. Ploog, Order-driven contribution to the planar hall effect in  $\text{Fe}_3\text{Si}$  thin films, *Phys. Rev. B* **71**, 172401 (2005).
- [6] B. T. Schaefer and K. C. Nowack, Electrically tunable and reversible magnetoelectric coupling in strained bilayer graphene, *Phys. Rev. B* **103**, 224426 (2021).
- [7] S. Nandy, G. Sharma, A. Taraphder, and S. Tewari, Chiral anomaly as the origin of the planar hall effect in weyl semimetals, *Phys. Rev. Lett.* **119**, 176804 (2017).
- [8] N. Kumar, S. N. Guin, C. Felser, and C. Shekhar, Planar hall effect in the weyl semimetal  $\text{gdptbi}$ , *Phys. Rev. B* **98**, 041103 (2018).
- [9] M.-X. Deng, H.-J. Duan, W. Luo, W. Y. Deng, R.-Q. Wang, and L. Sheng, Quantum oscillation modulated angular dependence of the positive longitudinal magnetoresistivity and planar hall effect in weyl semimetals, *Phys. Rev. B* **99**, 165146 (2019).
- [10] L. Li, J. Cao, C. Cui, Z.-M. Yu, and Y. Yao, Planar hall effect in topological weyl and nodal-line semimetals, *Phys. Rev. B* **108**, 085120 (2023).
- [11] D. Ma, H. Jiang, H. Liu, and X. C. Xie, Planar hall effect in tilted weyl semimetals, *Phys. Rev. B* **99**, 115121 (2019).
- [12] K. Das, S. K. Singh, and A. Agarwal, Chiral anomalies induced transport in weyl metals in quantizing magnetic field, *Phys. Rev. Res.* **2**, 033511 (2020).
- [13] Y.-W. Wei, J. Feng, and H. Weng, Spatial symmetry modulation of planar hall effect in weyl semimetals, *Phys. Rev. B* **107**, 075131 (2023).
- [14] K. Das and A. Agarwal, Linear magnetochiral transport in tilted type-i and type-ii weyl semimetals, *Phys. Rev. B* **99**, 085405 (2019).
- [15] S. Das, K. Das, and A. Agarwal, Chiral anomalies in three-dimensional spin-orbit coupled metals: Electrical, thermal, and gravitational anomalies, *Phys. Rev. B* **108**, 045405 (2023).
- [16] R. Ghosh and I. Mandal, Direction-dependent conductivity in planar hall set-ups with tilted weyl/multi-weyl semimetals, *Journal of Physics: Condensed Matter* **36**, 275501 (2024).
- [17] R. Ghosh and I. Mandal, Electric and thermoelectric response for weyl and multi-weyl semimetals in planar hall configurations including the effects of strain, *Physica E: Low-dimensional Systems and Nanostructures* **159**, 115914 (2024).
- [18] D. Rakhmilevich, F. Wang, W. Zhao, M. H. W. Chan, J. S. Moodera, C. Liu, and C.-Z. Chang, Unconventional planar hall effect in exchange-coupled topological insulator–ferromagnetic insulator heterostructures, *Phys. Rev. B* **98**, 094404 (2018).
- [19] S. Nandy, A. Taraphder, and S. Tewari, Berry phase theory of planar hall effect in topological insulators, *Scientific Reports* **8**, 14983 (2018).
- [20] D. Xiao, M.-C. Chang, and Q. Niu, Berry phase effects on electronic properties, *Rev. Mod. Phys.* **82**, 1959 (2010).
- [21] J. Cayssol and J. N. Fuchs, Topological and geometrical aspects of band theory, *Journal of Physics: Materials* **4**, 034007 (2021).
- [22] V. A. Zyuzin, In-plane hall effect in two-dimensional helical electron systems, *Phys. Rev. B* **102**, 241105 (2020).
- [23] J. H. Cullen, P. Bhalla, E. Marcellina, A. R. Hamilton, and D. Culcer, Generating a topological anomalous hall

- effect in a nonmagnetic conductor: An in-plane magnetic field as a direct probe of the berry curvature, *Phys. Rev. Lett.* **126**, 256601 (2021).
- [24] R. Battilomo, N. Scopigno, and C. Ortix, Anomalous planar hall effect in two-dimensional trigonal crystals, *Phys. Rev. Res.* **3**, L012006 (2021).
- [25] T. Liang, J. Lin, Q. Gibson, S. Kushwaha, M. Liu, W. Wang, H. Xiong, J. A. Sobota, M. Hashimoto, P. S. Kirchmann, Z.-X. Shen, R. J. Cava, and N. P. Ong, Anomalous hall effect in ZrTe<sub>5</sub>, *Nature Physics* **14**, 451 (2018).
- [26] J. Zhou, W. Zhang, Y.-C. Lin, J. Cao, Y. Zhou, W. Jiang, H. Du, B. Tang, J. Shi, B. Jiang, X. Cao, B. Lin, Q. Fu, C. Zhu, W. Guo, Y. Huang, Y. Yao, S. S. P. Parkin, J. Zhou, Y. Gao, Y. Wang, Y. Hou, Y. Yao, K. Suenaga, X. Wu, and Z. Liu, Heterodimensional superlattice with in-plane anomalous hall effect, *Nature* **609**, 46 (2022).
- [27] S. Sun, H. Weng, and X. Dai, Possible quantization and half-quantization in the anomalous hall effect caused by in-plane magnetic field, *Phys. Rev. B* **106**, L241105 (2022).
- [28] H. Wang, Y.-X. Huang, H. Liu, X. Feng, J. Zhu, W. Wu, C. Xiao, and S. A. Yang, Orbital origin of the intrinsic planar hall effect, *Phys. Rev. Lett.* **132**, 056301 (2024).
- [29] E. Drigo and R. Resta, Chern number and orbital magnetization in ribbons, polymers, and single-layer materials, *Phys. Rev. B* **101**, 165120 (2020).
- [30] D. Hara, M. S. Bahramy, and S. Murakami, Current-induced orbital magnetization in systems without inversion symmetry, *Phys. Rev. B* **102**, 184404 (2020).
- [31] K.-W. Kim, H. Jeong, J. Kim, and H. Jin, Vertical transverse transport induced by hidden in-plane berry curvature in two dimensions, *Phys. Rev. B* **104**, L081114 (2021).
- [32] D. L. Duong, S. J. Yun, and Y. H. Lee, van der waals layered materials: Opportunities and challenges, *ACS Nano* **11**, 11803–11830 (2017).
- [33] The Supplementary Material discusses: i) the derivation of planar-BC and planar-OMM expressions, ii) general expression for planar-BC and planar-OMM and analytical calculation of them for  $2 \times 2$  low-energy bilayer graphene model. iii) the detailed derivation of longitudinal and planar Hall response tensors, iv) the details of symmetry analysis, v) the strain implementation in the tight-binding model for bilayer graphene and  $y$  components of planar Berry curvature and OMM, vi) the Van Hove singularity and Lifshitz transition of Fermi surface, vii) estimation of planar Hall voltage, viii) comparison of planar Berry curvature and OMM for bilayer and trilayer graphene, and ix) other in-plane magneto-Hall responses in two-dimensional systems.
- [34] S.-C. Ho, C.-H. Chang, Y.-C. Hsieh, S.-T. Lo, B. Huang, T.-H.-Y. Vu, C. Ortix, and T.-M. Chen, Hall effects in artificially corrugated bilayer graphene without breaking time-reversal symmetry, *Nature Electronics* **4**, 116 (2021).
- [35] K. Das and A. Agarwal, Thermal and gravitational chiral anomaly induced magneto-transport in weyl semimetals, *Phys. Rev. Res.* **2**, 013088 (2020).
- [36] R. E. Newnham, *Properties of materials: anisotropy, symmetry, structure* (Oxford university press, 2005).
- [37] S. V. Gallego, J. Etxebarria, L. Elcoro, E. S. Tasci, and J. M. Perez-Mato, Automatic calculation of symmetry-adapted tensors in magnetic and non-magnetic materials: a new tool of the Bilbao Crystallographic Server, *Acta Crystallographica Section A* **75**, 438 (2019).
- [38] R.-C. Xiao, D.-F. Shao, W. Huang, and H. Jiang, Electrical detection of ferroelectriclike metals through the nonlinear hall effect, *Phys. Rev. B* **102**, 024109 (2020).
- [39] A. A. Taskin, H. F. Legg, F. Yang, S. Sasaki, Y. Kanai, K. Matsumoto, A. Rosch, and Y. Ando, Planar hall effect from the surface of topological insulators, *Nature Communications* **8**, 1340 (2017).
- [40] O. Breunig, Z. Wang, A. A. Taskin, J. Lux, A. Rosch, and Y. Ando, Gigantic negative magnetoresistance in the bulk of a disordered topological insulator, *Nature Communications* **8**, 15545 (2017).
- [41] P. He, S. S.-L. Zhang, D. Zhu, Y. Liu, Y. Wang, J. Yu, G. Vignale, and H. Yang, Bilinear magnetoelectric resistance as a probe of three-dimensional spin texture in topological surface states, *Nature Physics* **14**, 495–499 (2018).
- [42] B. Wu, X.-C. Pan, W. Wu, F. Fei, B. Chen, Q. Liu, H. Bu, L. Cao, F. Song, and B. Wang, Oscillating planar Hall response in bulk crystal of topological insulator Sn doped Bi<sub>1.1</sub>Sb<sub>0.9</sub>Te<sub>2</sub>S, *Applied Physics Letters* **113**, 011902 (2018).
- [43] P. He, S. S.-L. Zhang, D. Zhu, S. Shi, O. G. Heinonen, G. Vignale, and H. Yang, Nonlinear planar hall effect, *Phys. Rev. Lett.* **123**, 016801 (2019).
- [44] S.-H. Zheng, H.-J. Duan, J.-K. Wang, J.-Y. Li, M.-X. Deng, and R.-Q. Wang, Origin of planar hall effect on the surface of topological insulators: Tilt of dirac cone by an in-plane magnetic field, *Phys. Rev. B* **101**, 041408 (2020).
- [45] W. Rao, Y.-L. Zhou, Y.-j. Wu, H.-J. Duan, M.-X. Deng, and R.-Q. Wang, Theory for linear and nonlinear planar hall effect in topological insulator thin films, *Phys. Rev. B* **103**, 155415 (2021).
- [46] W. Ai, F. Chen, Z. Liu, X. Yuan, L. Zhang, Y. He, X. Dong, H. Fu, F. Luo, M. Deng, R. Wang, and J. Wu, Observation of giant room-temperature anisotropic magnetoresistance in the topological insulator  $\beta$ -ag<sub>2</sub>te, *Nature Communications* **15**, 1259 (2024).
- [47] Z. Zheng, Q. Ma, Z. Bi, S. de la Barrera, M.-H. Liu, N. Mao, Y. Zhang, N. Kiper, K. Watanabe, T. Taniguchi, J. Kong, W. A. Tisdale, R. Ashoori, N. Gedik, L. Fu, S.-Y. Xu, and P. Jarillo-Herrero, Unconventional ferroelectricity in moiré heterostructures, *Nature* **588**, 71 (2020).
- [48] X. Wang, K. Yasuda, Y. Zhang, S. Liu, K. Watanabe, T. Taniguchi, J. Hone, L. Fu, and P. Jarillo-Herrero, Interfacial ferroelectricity in rhombohedral-stacked bilayer transition metal dichalcogenides, *Nature Nanotechnology* **17**, 367 (2022).
- [49] K. Yasuda, X. Wang, K. Watanabe, T. Taniguchi, and P. Jarillo-Herrero, Stacking-engineered ferroelectricity in bilayer boron nitride, *Science* **372**, 1458 (2021).